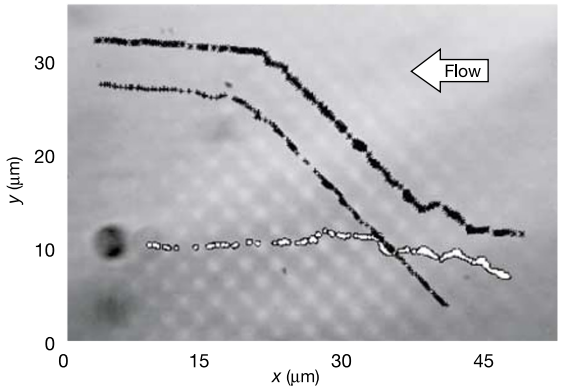

Figure 4 Optical fractionation by size. Black crosses represent the frame-by-frame positions (tracked at standard video rates with ~8 nm precision) of two 2-μm diameter protein microcapsules (drug delivery agents) as they flow from right to left across the optical lattice. The flow speed is 20 μm s^{-1} with a total incident laser power of 530 mW. Again, significant angular deflection is achieved, while a co-flowing 4-μm-diameter capsule of the same sort flows nearly straight through (white dots). The collection of 2-μm capsules allows a controlled study of drug delivery at the cellular level.

of the lattice. Such anisotropy merely changes a prefactor in term (1), for motion along the direction of lowered barrier heights.

We note that it is necessary to move beyond the limit of discrete, isotropic traps to achieve the sorts of concentrated, mixed-flow separations demonstrated here. Rather than using kinetic lock-in of hopping probabilities[4], we provide a more deterministic form of channelling. We use light patterns that contain a tailored degree of 'interconnectedness' (that is, lower potential energy barriers) along the direction of desired channelling[1]. Supplementary Fig. B provides details of the experimental parameters used to tune these linkages, along with detailed mapping of lattice parameters and the linkages themselves. The details of the linkages between lattice sites plays a key role in optical fractionation. Distinct individual lattice points are ideally suited to trapping particles, whereas interlinks between the lattice sites are central to deflecting particles into a desired trajectory. The optimum lattice for fractionation with high angles of displacement lies between a discrete lattice of intensity maxima and continuous guides; we went on to find that the body-centred tetragonal (b.c.t.) lattice, used for the results shown in Figs 2–4, is satisfactory. This is demonstrated clearly in Supplementary Fig. D, where the linked b.c.t. lattice has both the highest efficiency and the highest throughput when fractionating at 45°. More detailed calculations and discussion of this will appear elsewhere[18].

Arrays composed of discrete, isotropic traps tend to 'jam' (which is why studies involving such arrays tend to use extremely dilute flows). The dwell time in strongly localizing traps significantly slows particles with respect to the input stream. Jamming is likely to occur in long arrays of this type, effectively preventing particles that would otherwise pass through un-deflected from doing so, and leading to 'spill-over' contamination of the uptake stream.

Practical fractionating arrays must be long enough to transport the selected particles (transversely) from the most distant portion of the input stream all the way to the uptake stream, where they are extracted. For dense flows, greater length is required, but in general the larger the angle of deflection through the lattice, the shorter the lattice can be, making fractionation at 45° with a linked b.c.t. lattice particularly well suited to practical implementation of optical fractionation. □

Received 1 July; accepted 21 October 2003; doi:10.1038/nature02144.

1. Tatarkova, S. A., Sibbett, W. & Dholakia, K. Brownian particle in an optical potential of the washboard type. *Phys. Rev. Lett.* **91,** 038101 (2003).
2. Ashkin, A., Dziedzic, J. M., Bjorkholm, J. E. & Chu, S. Observation of a single-beam gradient force optical trap for dielectric particles. *Opt. Lett.* **11,** 288–290 (1986).
3. Burns, M. M., Fournier, J. M. & Golovchenko, J. A. Optical matter—crystallization and binding in intense optical-fields. *Science* **249,** 749–754 (1990).
4. Korda, P. T., Taylor, M. B. & Grier, D. G. Kinetically locked-in colloidal transport in an array of optical tweezers. *Phys. Rev. Lett.* **89,** 128301 (2002).
5. Fu, A. Y., Spence, C., Scherer, A., Arnold, F. H. & Quake, S. R. A microfabricated fluorescence-activated cell sorter. *Nature Biotechnol.* **17,** 1109–1111 (1999).
6. Han, J. & Craighead, H. G. Separation of long DNA molecules in a microfabricated entropic trap array. *Science* **288,** 1026–1029 (2000).
7. Nykypanchuk, D., Strey, H. H. & Hoagland, D. A. Brownian motion of DNA confined within a two-dimensional array. *Science* **297,** 987–990 (2002).
8. Ertas, D. Lateral separation of macromolecules and polyelectrolytes in microlithographic arrays. *Phys. Rev. Lett.* **80,** 1548–1551 (1998).
9. Duke, T. A. J. & Austin, R. H. Microfabricated sieve for the continuous sorting of macromolecules. *Phys. Rev. Lett.* **80,** 1552–1555 (1998).
10. Chou, C. F. *et al.* Electrodeless dielectrophoresis of single- and double-stranded DNA. *Biophys. J.* **83,** 2170–2179 (2002).
11. Galbraith, D. W., Anderson, M. T. & Herzenberg, L. A. in *Methods in Cell Biology* Vol. 58 (eds Sullivan, K. F. & Kay, S. A.) 315–341 (Academic, London, 1999).
12. Athanasopoulou, A., Koliadima, A. & Karaiskakis, G. New methodologies of field-flow fractionation for the separation and characterization of dilute colloidal samples. *Instrum. Sci. Technol.* **24,** 79–94 (1996).
13. Dholakia, K., Spalding, G. C. & MacDonald, M. Optical tweezers: The next generation. *Phys. World* **15,** 31–35 (2002).
14. MacDonald, M. P. *et al.* Creation and manipulation of three-dimensional optically trapped structures. *Science* **296,** 1101–1103 (2002).
15. Greiner, M., Mandel, O., Esslinger, T., Hansch, T. W. & Bloch, I. Quantum phase transition from a superfluid to a Mott insulator in a gas of ultracold atoms. *Nature* **415,** 39–44 (2002).
16. Korda, P. T., Spalding, G. C. & Grier, D. G. Evolution of a colloidal critical state in an optical pinning potential landscape. *Phys. Rev. B* **66,** 024504 (2002).
17. Crocker, J. C. & Grier, D. G. Methods of digital video microscopy for colloidal studies. *J. Colloid Interface Sci.* **179,** 298–310 (1996).
18. MacDonald, M. P., Spalding, G. C. & Dholakia, K. Transport and fractionation of brownian particles in an optical lattice. *Phys. Rev. Lett.* (submitted).
19. Imasaka, T., Kawabata, Y., Kaneta, T. & Ishidzu, Y. Optical chromatography. *Anal. Chem.* **67,** 1763–1765 (1995).
20. Marmottant, P. & Hilgenfeldt, S. Controlled vesicle deformation and lysis by single oscillating bubbles. *Nature* **423,** 153–156 (2003).

Supplementary Information accompanies the paper on **www.nature.com/nature**.

Acknowledgements We thank P. Campbell for supplying protein microcapsules, and A. Riches for blood samples. This work was supported by the UK Engineering and Physical Sciences Research Council, the Research Corporation, and the National Science Foundation.

Competing interests statement The authors declare that they have no competing financial interests.

Correspondence and requests for materials should be addressed to M.P.M. (mpm4@st-and.ac.uk).

Low-temperature processing of 'baroplastics' by pressure-induced flow

Juan A. Gonzalez-Leon[1], Metin H. Acar[1], Sang-Woog Ryu[1], Anne-Valérie G. Ruzette[1]* & Anne M. Mayes[1]

[1]*Department of Materials Science and Engineering, Massachusetts Institute of Technology, 77 Massachusetts Avenue, Cambridge, Massachusetts 02139, USA*

* Present address: Laboratoire Matiére Molle et Chimie, ESPCI, 10 rue Vauquelin, F-75231 Paris cedex 05, France

The manufacturing of plastics traditionally involves melt processing at temperatures typically greater than 200 °C—to enable extrusion or moulding under pressure into desired forms—followed by solidification. This process consumes energy and can cause substantial degradation of polymers and additives (such as flame retardants and ultraviolet stabilizers), limiting plastics performance and recyclability[1]. It was recently reported that the application of pressure could induce melt-like behaviour in the block copolymer polystyrene-*block*-poly(*n*-butyl methacrylate) (PS-*b*-PBMA)[2], and this behaviour has now been demon-

strated in a range of other block copolymer systems[3–8]. These polymers have been termed baroplastics[2–5]. However, in each case, the order-to-disorder transition, which gives rise to the accompanying change in rheology from soft solid to melt[9,10], was observed at temperatures far exceeding the glass transition temperatures (T_g) of both components. Here we show that baroplastic systems containing nanophase domains of one high-T_g and one low-T_g component can exhibit melt-like flow under pressure at ambient temperature through an apparent semi-solid partial mixing mechanism that substantially preserves the high-T_g phase. These systems were shredded and remoulded ten times with no evident property degradation. Baroplastics with low-temperature formability promise lower energy consumption in manufacture and processing, reduced use of additives, faster production and improved recyclability, and also provide potential alternatives to current thermoplastic elastomers, rubber-modified plastics, and semi-crystalline polymers[11,12].

To design materials molecularly, incorporating a low-T_g component that can solvate (or partially solvate) a high-T_g component under pressure, we employed principles for polymer pair miscibility recently elucidated through a straightforward extension of the Flory–Huggins regular solution model for polymer mixtures to compressible systems[4,13,14]. The free energy per unit volume of a binary compressible polymer mixture can be written as:

$$\Delta g_{\mathrm{mix}} = kT\left[\frac{\phi_A\tilde{\rho}_A}{N_A\nu_A}\ln\phi_A + \frac{\phi_B\tilde{\rho}_B}{N_B\nu_B}\ln\phi_B\right] + \phi_A\tilde{\rho}_A\phi_B\tilde{\rho}_B(\delta_{A,0}-\delta_{B,0})^2 + \phi_A\phi_B(\tilde{\rho}_A-\tilde{\rho}_B)(\delta_A^2-\delta_B^2) \quad (1)$$

where k is the Boltzmann constant; ϕ_i, N_i, and ν_i are the volume fraction, number of segments per chain, and hard core segmental volume of the ith component; $\delta_{i,0}^2$ and δ_i^2 are the cohesive energy densities at 0 K and temperature T, respectively; and $\tilde{\rho}_i = \rho_i/\rho_i^*$ is the reduced density, with the hard core density defined as $\rho_i^* = M_{u,i}/N_0\nu_i$, where $M_{u,i}$ is the monomer molecular mass and N_0 is Avogadro's number. In equation (1), the first two terms are analogous to the Flory–Huggins entropy (−) and enthalpy (+) of mixing terms, while the third term arises solely from compressibility. The third term can either favour (−) or oppose (+) segmental mixing, tending to zero in the incompressible limit. Equation (1) can be used to predict phase diagrams solely from pure component properties, and has successfully captured the qualitative phase behaviour of over 30 weakly interacting polymer pairs[4,13,14]. In the present context, systems for which the third term approaches zero at 0 K from negative values, and whose ambient-state densities nearly match[15] ($0.94\ \rho_A < \rho_B < 1.06\ \rho_A$), have been found to exhibit pressure-induced miscibility, including PS/PBMA[2], PS/poly(hexyl methacrylate)[3,4], PS/poly(pentyl methacrylate)[5], polybutadiene/polyisoprene (PB/PI)[8] and poly(ethylene propylene)/poly(ethyl methylene) (PEP/PEE)[9]. By contrast, these conditions are not met for PS/PI or PS/PB, two commercially important block copolymer systems that have been found to exhibit reduced miscibility with applied pressure[16–19]. Using the above criteria, two new baroplastic candidates with one high-T_g and one low-T_g component were identified, namely, polystyrene/poly(*n*-butyl acrylate) (PS/PBA, $T_{g,PBA} \approx -54\,^{\circ}C$) and polystyrene/poly(2-ethylhexyl acrylate) (PS/PEHA, $T_{g,PEHA} \approx -50\,^{\circ}C$). Table 1 lists the molecular and compositional characteristics of the materials discussed in this study.

The ability to process PS-*b*-PBA and PS-*b*-PEHA block copolymers at room temperature despite their high-T_g PS component was demonstrated by compression-moulding the freeze-dried precipitates into rigid transparent objects using a standard hydraulic press and moulds machined from stainless steel or aluminium. Figure 1a shows the starting material and final products of a 38,000 g mol^{-1} PS-*b*-PBA block copolymer incorporating 45 wt% PBA moulded at 25 °C and 34.5 MPa (5,000 p.s.i.) for 5 min. The transparency of the moulded objects and their accuracy of form are testimony that the copolymer flowed under applied pressure to take the shape of its

Table 1 **Molecular and compositional characteristics of baroplastics**

System	PS (wt%)*	Molecular mass, M_n (g mol^{-1})†	Average size (nm)‡
Block copolymers			
PS-*b*-PBA	70	100,000	
PS-*b*-PBA	63	73,000	
PS-*b*-PBA	55	38,000	
PS-*b*-PEHA	48	60,000	
Core–shell			
PEHA/PS	50	300,000/200,000	67
PBA/ PS-d_8	66	320,000/120,000	87

*Determined by ^{1}H-NMR.
†Molecular weight measured by GPC based on PS standard.
‡Particle size determined by dynamic light scattering using a Brookhaven Instruments Co. Zeta Potential Analyzer.

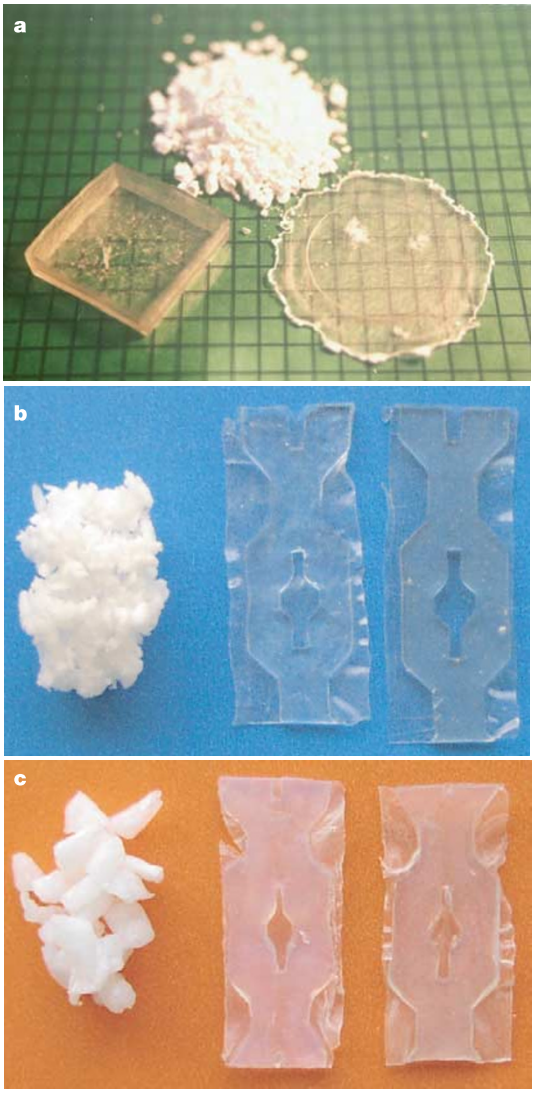

Figure 1 Processed baroplastics samples. **a**, 38,000 g mol^{-1} polystyrene-*block*-poly(*n*-butyl acrylate), PS-*b*-PBA, with 45 wt% PBA as obtained from freeze-drying and after processing by compression moulding at 25 °C using a pressure of 34.5 MPa (5,000 p.s.i.). **b**, 60,000 g mol^{-1} polystyrene-*block*-poly(2-ethylhexyl acrylate), PS-*b*-PEHA, with 52 wt% PEHA reprocessed once and ten times at 30 °C under a pressure of 34.5 MPa. **c**, PEHA/PS core–shell material with 52 wt% PEHA processed one time and recycled ten times at 25 °C with a pressure of 34.5 MPa.

container. For example, the lid of a plastic sample holder box was copied to sufficient accuracy to provide a tight seal with the original box. A 73,000 g mol^{-1} PS-*b*-PBA sample containing 27 wt% PBA could be processed at 80 °C at 34.5 MPa.

The premise that low-temperature processing capability arises from the pressure-enhanced miscibility of the PS and PBA block components is supported by *in situ* small-angle neutron scattering (SANS) data taken at elevated temperatures (120 °C $< T <$ 200 °C) on a 100,000 g mol^{-1} PS-*b*-PBA system with 70 wt% PS (data not shown). A pressure coefficient of $dT_{ODT}/dP \approx -100$ °C kbar^{-1} was estimated[2] for this material, which disorders with increasing temperature (ODT, order to disorder transition).

Moulding studies on a 60,000 g mol^{-1} PS-*b*-PEHA block copolymer incorporating 52 wt% PEHA similarly revealed low-temperature processing capability, and further illustrated the recycling potential of baroplastic block copolymers. Figure 1b shows moulded samples reprocessed once and ten times at 34.5 MPa and 30 °C for 5 min. Between consecutive mouldings, samples were shredded into ~3 mm pieces to create the feed. Although detailed measurements have not been performed to date, the mechanical and optical properties (discounting particulate inclusions) after ten moulding operations appear comparable to the original moulded specimen.

To probe how low-temperature processing influences morphology, SANS was performed on samples before and after room-temperature processing. Figure 2a shows SANS data for the same PS-*b*-PEHA block copolymer in its initial freeze-dried state and after processing once and ten times at 34.5 MPa and 25 °C for 5 min. The sample before moulding shows a sharp reflection at wavevector $q \approx 0.025$ Å^{-1}, denoting the nanoscale separation of the PS and PEHA blocks with a periodicity of 25 nm. After processing, the scattering maximum is observed to broaden and decrease in intensity, suggesting that the PS and PEHA blocks are made at least partially miscible under pressure.

Differential scanning calorimetry (DSC) traces on this same material freeze-dried and after ten recycles at 25 °C are shown in Fig. 3a. Two glass transitions are observed in each sample near −36 and 55 °C. The fact that the material continues to exhibit a glassy-phase T_g well above the processing temperature of 25 °C is an interesting clue to the processing mechanism. One would expect that if the copolymer were driven into the fully disordered state during moulding, upon the removal of pressure, demixing of the blocks would be arrested kinetically, that is, when the glass transition of the forming glassy phase equals the processing temperature. Instead, the glassy-state T_g remains well above the processing temperature—a clear advantage for applications. A likely explanation is that the copolymer does not fully disorder under pressure, but instead retains some glassy regions, processing as a semi-solid.

This view of the baroplastics processing mechanism is supported by experiments on a PS-*b*-PEHA sample processed at 34.5 MPa that was subsequently annealed at 85 °C overnight and reprocessed at 34.5 MPa. SANS data for the processed, annealed and reprocessed samples are shown in Fig. 2b. Upon annealing, the scattering maximum intensifies and narrows, indicative of enhanced block demixing and/or domain order. The corresponding DSC trace (Fig. 3b) shows the emergence of a glass transition at ~85 °C, with the glass transitions at −35 and 55 °C still present. After remoulding, the peak in the SANS data reverts back to the shape characteristic of the processed state. The DSC trace, however, shows that this sample retains regions with a $T_g \approx 85$ °C—that is, 60° above the processing temperature. The fact that these regions are not seen in the initially processed sample, but only after the elevated temperature annealing, provides strong supporting evidence for a semi-solid processing mechanism where the high-T_g phase is retained.

The low-temperature processing of block copolymers is thought to be facilitated by their morphology, which presents a high degree of interface between the two polymer components. From a commercial viewpoint, however, block copolymers have potential drawbacks as substitutes for today's commodity plastics in that their synthesis is generally more complex and expensive, while the number of polymers that can be readily incorporated into block copolymers is limited[20–22]. As an alternative approach to the preparation of baroplastics, core–shell nanoparticle systems were investigated. Similar to block copolymer nanophases, core–shell nanoparticles contain domains of one component that are molecularly adjacent to those of the second component. Such systems can be made by emulsion polymerization of sequentially added monomers[23], as performed here, or by emulsification and surface precipitation of previously synthesized polymers, allowing for a substantially wider array of baroplastics candidates.

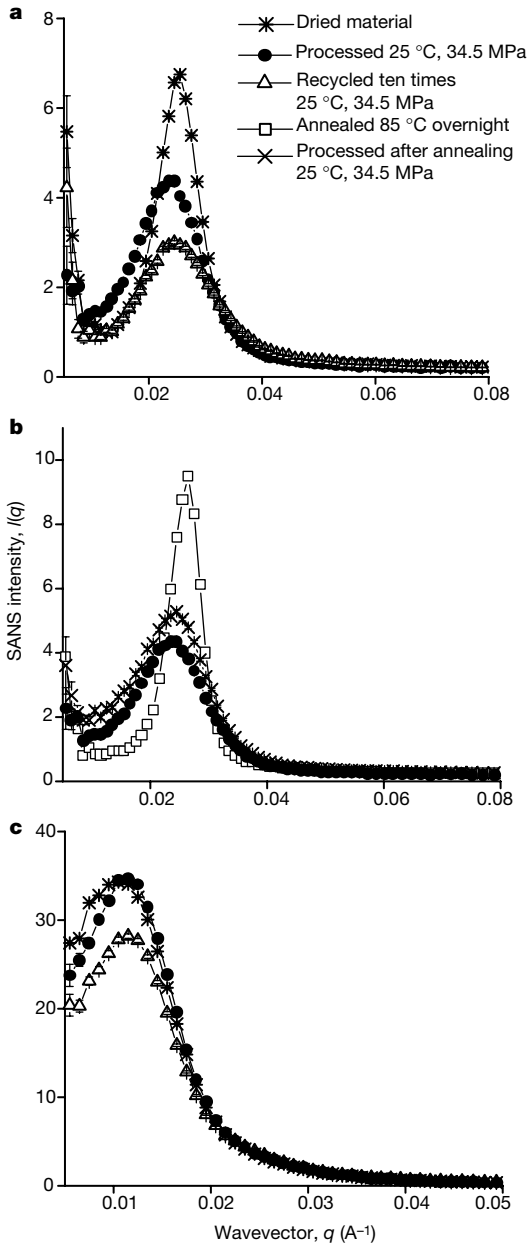

Figure 2 Small-angle neutron scattering intensity, $I(q)$, versus wavevector, q, plots. **a**, **b**, 60,000 g mol^{-1} polystyrene-*block*-poly(2-ethylhexyl acrylate), PS-*b*-PEHA, with 52 wt% PEHA and the indicated processing conditions. **c**, PEHA/PS core–shell with 50 wt% PEHA and the indicated processing conditions.

Core–shell nanoparticles with one glassy and one rubbery component have been exploited as coatings[24,25] and as impact-modifying additives for plastics (with a crosslinked rubbery core)[26]. To create systems that could be moulded as bulk plastics by pressure-induced mixing, we synthesized core–shell nanoparticles consisting of a non-crosslinked, low-T_g core polymer and a high-T_g shell polymer.

The baroplastic properties of PEHA/PS core–shell nanoparticles with 50 wt% polystyrene and average particle diameter of 67 nm are demonstrated in Fig. 1c, depicting a compression-moulded specimen processed at 34.5 MPa for 5 min at 25 °C from the dried state and one reprocessed ten times following the procedure described above. Similar to the PS-*b*-PEHA block copolymer, the core–shell material can be readily remoulded at room temperature after repeated processing operations, an effect that we propose derives from the pressure-induced partial miscibilization of the PEHA and PS components.

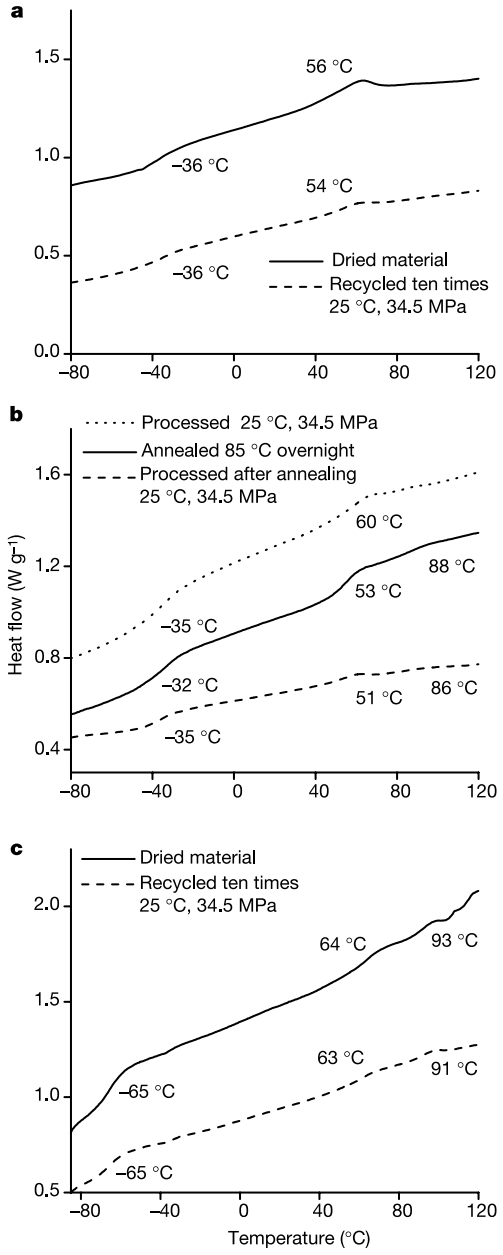

Figure 3 Heat flow versus temperature traces from differential scanning calorimetry, DSC. **a**, **b**, polystyrene-*block*-poly(2-ethylhexyl acrylate), PS-*b*-PEHA, with the indicated processing conditions. **c**, PEHA/PS core–shell with 50 wt% PEHA and the indicated processing conditions. Measurements were performed on a TA Instruments Q1000 DSC at a 5 °C min^{-1} rate.

SANS data for the PEHA/PS nanoparticle system in the as-dried state, after one moulding operation and after ten recycles are shown in Fig. 2c. Several important features are notable. First, each data set exhibits a broad maximum characteristic of the interparticle spacing, suggesting that, similar to block copolymer baroplastics, the initial sample morphology is substantially preserved during low-temperature processing. Upon the initial moulding, the peak position shifts to a slightly larger wavevector. This behaviour was found for all the core–shell systems studied and reflects the material's densification under compression. With further processing, the peak position remains constant but its amplitude diminishes, suggesting enhanced mixing and a corresponding loss of contrast between PS and PEHA domains. This latter result is strong evidence that PS/PEHA indeed exhibits the predicted pressure-induced miscibility.

DSC data on this core–shell system are consistent with a semi-solid processing mechanism. Figure 3c shows DSC traces for the as-dried material and the specimen recycled ten times. Three glass transitions are apparent in each data set, at −65, 93 and 64 °C, corresponding to the PEHA, PS and interphase regions, respectively. (A fourth T_g may be weakly present for both samples near −35 °C.) The fact that little variation is observed in these traces after ten recycles suggests that the system does not undergo wholesale mixing under pressure, but instead flows and forms as a semi-solid.

Although processing kinetics were not a focus of this initial investigation, a preliminary study of the effects of processing time on morphology were performed on a PBA/PS-d_8 core–shell nanoparticle system with 66 wt% PS-d_8 and an average particle diameter of 87 nm. SANS data for this system processed at 34.5 MPa and 25 °C for 1, 10 and 30 min show a reduction in the peak intensity with time (not shown), indicating the PS-d_8 and PBA components become increasingly intermixed. DSC traces for this system processed for 1 and 30 min again show three T_g values near −40, 90 and 47 °C, corresponding to the PBA, PS and interphase regions of the particles, respectively. For this material, the mixed-state T_g can be estimated from the components T_g and their mass fractions, w, from $1/T_{g,mix} = w_1/T_{g,1} + w_2/T_{g,2}$ to be 28 °C — effectively eliminating a processing mechanism that involves complete mixing of the two components.

As controls, PS/PI block copolymers and core–shell nanoparticles were also investigated, to confirm that the low-temperature processing capability witnessed in our investigations had its origins in the pressure-enhanced miscibility of the systems studied. The application of pressure is known to reduce the miscibility of PS/PI[16–18], allowing us to separate structural and kinetic effects from thermodynamics. Attempts to compression-mould a commercial PS-*b*-PI-*b*-PS triblock copolymer with 22 wt% PS and $M_n = 90{,}000$ g mol^{-1} at 25 °C and 55 °C were unsuccessful. Interestingly, a PI/PS core–shell nanoparticle system having 62 wt% PS and total average diameter of 29 nm could be processed into transparent films from the dried precipitate; however, the product was easily fractured and showed poor cohesion during attempts to reprocess.

In summary, we have demonstrated moulding of baroplastic block copolymers and core–shell nanoparticles comprising one glassy and one rubbery component, solely by applying pressure. Capitalizing on pressures typically experienced in plastics manufacturing operations such as injection- and compression-moulding, baroplastics processing may be feasible using current manufacturing equipment. The molecular mechanism underlying this phenomenon appears to involve pressure-induced partial intermixing of dissimilar nanophase domains, resulting in a semi-solid state that facilitates moulding. Such a semi-solid forming operation could be compared to semi-solid metals casting processes that allow for rapid, high-precision alloy castings from slurries or billets

with solids content as high as 40–50% (ref. 27).

As a new paradigm for plastics manufacturing, semi-solid processing of baroplastics raises prospects for the low-temperature moulding of plastics incorporating high-T_g, crystallizing or inorganic components, wherein such hard phases move within a fluidized baroplastic medium. We are currently investigating such systems. By removing the resin-heating and mould-cooling requirements, pressure-based processing could decrease both energy consumption and manufacturing time, while eliminating the thermooxidative degradation that limits plastics recyclability. □

Methods

Block copolymer synthesis

Block copolymers of PS-*b*-PBA and PS-*b*-PEHA were synthesized by atom transfer radical polymerization (ATRP)[20,28,29]. The polystyrene block was first polymerized using methyl-2-bromo-propionate as initiator and CuCl/N,N,N′,N′,N″-pentamethyldiethylene triamine as the catalyst complex in toluene solution at 100 °C. Once the styrene polymerization reached completion, the temperature was lowered to 80 °C and acrylate monomer was added to obtain the second block. The resulting polymer solution was then passed through an alumina column to remove the catalyst and the copolymer precipitated in methanol. The recovered block copolymers were purified by repeated dissolution in dichloromethane followed by precipitation in methanol. The materials were then dried under vacuum followed by freeze-drying from benzene overnight. Compositions and molecular weights of the resulting block copolymers were determined using ^{1}H nuclear magnetic resonance (NMR) and gel permeation chromatography (GPC) based on polystyrene standards.

Core–shell nanoparticle synthesis

Core–shell nanoparticles of PEHA/PS and PBA/PS-d_8 were synthesized by a two-stage microemulsion polymerization technique[23,26]. Tetradecyltrimethylammonium bromide and 2,2′-azobis(2-methylpropionamidine) dihydrochloride were used as emulsifier and initiator, respectively. Polymerization was performed under nitrogen at 65 °C. Acrylate monomer was first added slowly to dionized water in the presence of emulsifier with vigorous stirring and reacted for 15 h. Pre-emulsified styrene was then added slowly to this solution and allowed to react for 3 h. The resulting core–shell particles were precipitated in methanol/water (with a trace amount of NaCl) and washed in DI water several times. The product was then vacuum-dried in the presence of phosphorus pentoxide for three days at room temperature. Compositions and molecular masses were determined as above. Average particle sizes were determined by dynamic light scattering using a Brookhaven Instruments Co. Zeta Potential Analyzer fitted with a 676-nm laser source.

SANS

Measurements were performed at The Manuel Lujan Jr. Neutron Scattering Center at Los Alamos National Laboratory on the Low-*Q* diffractometer, LQD, with the following instrument configuration: wavelength = 1.5–15 Å at 20 Hz, scattering angle = 6–60 mrad on a 59-cm diameter detector, resulting in a q range of 0.003–0.5 Å^{-1}. Samples were ~1-cm-diameter disks of variable thickness. Scattered intensities were corrected for background and thickness in the standard manner.

Received 21 March; accepted 21 October 2003; doi:10.1038/nature02140.

1. Herbst, H., *et al.* in *Frontiers in the Science and Technology of Recycling* (ed. Akovali, G.) 73–101 (Kluwer Academic, Dordrecht, The Netherlands, 1997).
2. Pollard, M., Russell, T. P., Ruzette, A. V., Mayes, A. M. & Gallot, Y. The effect of hydrostatic pressure on the lower critical ordering transition in diblock copolymers. *Macromolecules* **31,** 6493–6498 (1998).
3. Ruzette, A.-V. G., Mayes, A. M., Pollard, M., Russell, T. P. & Hammouda, B. Pressure effects on the phase behavior of styrene/n-alkyl methacrylate block copolymers. *Macromolecules* **36,** 3351–3356 (2003).
4. Ruzette, A.-V. G., Banerjee, P., Mayes, A. M. & Russell, T. P. A simple model for baroplastic behavior in block copolymer melts. *J. Chem. Phys.* **114,** 8205–8209 (2001).
5. Ryu, D. Y., Lee, D. J., Kim, J. K., Lavery, K. A. & Russell, T. P. Effect of hydrostatic pressure on closed-loop phase behavior of block copolymers. *Phys. Rev. Lett.* **90,** 235501 (2003).
6. Hasegawa, H. *et al.* Small-angle neutron scattering studies on phase behavior of block copolymers. *J. Phys. Chem. Solids* **60,** 1307–1312 (1999).
7. Frielinghaus, H., Schwahn, D., Mortensen, K., Almdal, K. & Springer, T. Composition fluctuations and coil conformations in a poly(ethylene-propylene)-poly(ethyl ethylene) diblock copolymer as a function of temperature and pressure. *Macromolecules* **29,** 3263–3271 (1996).
8. Schwahn, D., Frielinghaus, H., Mortensen, K. & Almdal, K. Temperature and pressure dependence of the order parameter fluctuations, conformational compressibility, and the phase diagram of the PEP-PDMS diblock copolymer. *Phys. Rev. Lett.* **77,** 3153–3156 (1996).
9. Russell, T. P., Karis, T. E., Gallot, Y. & Mayes, A. M. Lower critical ordering transition in a diblock copolymer melt. *Nature* **368,** 729–731 (1994).
10. Ryu, D. Y., Jeong, U., Kim, J. K. & Russell, T. P. Closed-loop phase behaviour in block copolymers. *Nature Mater.* **1,** 114–117 (2002).
11. Holden, G. *et al.* in *Thermoplastic Elastomers* (ed. Holden, G.) 573–599 (Hanser, Munich/Vienna/New York, 1996).
12. Ehrenstein, G. H. *Polymeric Materials* 63–89, 98–116 (Hanser, Munich, 2001).
13. Ruzette, A.-V. G. & Mayes, A. M. A simple free energy model for weakly interacting polymer blends. *Macromolecules* **34,** 1894–1907 (2001).
14. Gonzalez-Leon, J. A. & Mayes, A. M. Phase behavior prediction of ternary polymer mixtures. *Macromolecules* **36,** 2508–2515 (2003).
15. Ruzette, A.-V. G. *et al.* Phase behavior of diblock copolymers between styrene and n alkyl methacrylates. *Macromolecules* **31,** 8509–8517 (1998).
16. Hajduk, D. A., Urayama, P., Gruner, S. M. & Erramilli, S. High-pressure effects on the disordered phase of block copolymer melts. *Macromolecules* **28,** 7148–7156 (1995).
17. Hajduk, D. A., Gruner, S. M., Erramilli, S., Register, R. A. & Fetters, L. J. High-pressure effects on the order/disorder transition in block copolymer melts. *Macromolecules* **29,** 1473–1481 (1996).
18. Steinhoff, B. *et al.* Pressure dependence of the order-to-disorder transition in polystyrene/polyisoprene and polystyrene/ poly(methylphenylsiloxane) diblock copolymers. *Macromolecules* **31,** 36–40 (1998).
19. Migler, K. B. & Han, C. C. Static and kinetic study of a pressure-induced order-disorder transition: birefringence and neutron scattering. *Macromolecules* **31,** 300–305 (1998).
20. Patten, T. E. & Matyjaszewski, K. Atom transfer radical polymerization and the synthesis of polymeric materials. *Adv. Mater.* **10,** 901–915 (1998).
21. Malmstrom, E. E. & Hawker, C. J. Macromolecular engineering via 'living' free radical polymerizations. *Macromol. Chem. Phys.* **199,** 923–935 (1998).
22. Hillmyer, M. Block copolymer synthesis. *Curr. Opin. Solid State Mater. Sci.* **4,** 559–564 (1999).
23. Ha, J. W., Park, I. J., Lee, S. B. & Kim, D. K. Preparation and characterization of core–shell particles containing perfluoroalkyl acrylate in the shell. *Macromolecules* **35,** 6811–6818 (2002).
24. Keddie, J. L. Film formation of latex. *Mater. Sci. Eng. R* **21,** 101–170 (1997).
25. Dos Santos, F. D. & Leibler, L. Large deformation films from soft-core/hard-shell hydrophobic latexes. *J. Polym. Sci. B* **41,** 224–234 (2003).
26. Lovell, P. A. & Pierre, D. in *Emulsion Polymerization and Emulsion Polymers* (eds Lovell, P. A. & Aasser, M. S.) 657–695 (John Wiley & Sons, New York, 1997).
27. Flemings, M. C. Behavior of metal alloys in the semisolid state. *Metall. Trans. B* **22,** 269–293 (1991).
28. Shipp, D. A., Wang, J.-L. & Matyjaszewski, K. Synthesis of acrylate and methacrylate block copolymers using atom transfer radical polymerization. *Macromolecules* **31,** 8005–8008 (1998).
29. Cassebras, M., Pascual, S., Polton, A., Tardi, M. & Vairon, J. P. Synthesis of di- and triblock copolymers of styrene and butyl acrylate by controlled atom transfer radical polymerization. *Macromol. Rapid Commun.* **20,** 261–264 (1999).

Acknowledgements We acknowledge the support of the Seaver Institute, the Lord Foundation, Lord Corporation, the MRSEC Program of the National Science Foundation and the Office of Naval Research. This work benefited from the use of the Los Alamos Neutron Science Center at the Los Alamos National Laboratory, funded by the US Department of Energy.

Competing interests statement The authors declare that they have no competing financial interests.

Correspondence and requests for materials should be addressed to A.M.M. (amayes@mit.edu).

Synthetic design of crystalline inorganic chalcogenides exhibiting fast-ion conductivity

Nanfeng Zheng[1], Xianhui Bu[2]* & Pingyun Feng[1]

[1]*Department of Chemistry, University of California, Riverside, California 92521, USA*
[2]*Department of Chemistry, University of California, Santa Barbara, California 93106, USA*

* Present address: Department of Chemistry and Biochemistry, California State University, 1250 Bellflower Blvd, Long Beach, California 90840, USA

Natural porous solids such as zeolites are invariably formed with inorganic cations such as Na^+ and K^+ (refs 1, 2). However, current research on new porous materials is mainly focused on the use of organic species as either structure-directing or structure-building units; purely inorganic systems have received relatively little attention in exploratory synthetic work[3–9]. Here we report the synthesis of a series of three-dimensional sulphides and selenides containing highly mobile alkali metal cations as charge-balancing extra-framework cations. Such crystalline inorganic chalcogenides integrate zeolite-like architecture with high anionic framework polarizability and high concentrations of mobile cations. Such structural features are particularly desirable for the development of fast-ion conductors[10]. These materials demonstrate high ionic conductivity (up to 1.8×10^{-2} ohm^{-1} cm^{-1}) at room temperature and moderate to high humidity. This synthetic methodology, together with novel

